Duality of Nrf2 in iron-overload cardiomyopathy

Enrica Federti,[1] Francesca Vinchi,[2,3] Iana Iatcenko,[1] Alessandra Ghigo,[4] Alessandro Matte,[1] Serge Cedrick Mbiandjeu Toya,[1] Angela Siciliano,[1] Deborah Chiabrando,[4] Emanuela Tolosano,[4] Steven Zebulon Vance,[2] Veronica Riccardi,[1] Immacolata Andolfo,[5,6] Manuela Iezzi,[7] Alessia Lamolinara,[7] Achille Iolascon[5,6] and Lucia De Franceschi[1]

[1]Department of Medicine, University of Verona and AOUI Verona, Verona, Italy; [2]Iron Research Laboratory, Lindsley Kimball Research Institute, New York Blood Center, New York, NY, USA; [3]Department of Pathology and Laboratory Medicine, Weill Cornell Medicine, New York, NY; [4]Department Molecular Biotechnology and Health Sciences, Molecular Biotechnology Center "Guido Tarrone", University of Torino, Torino, Italy; [5]Department of Molecular Medicine and Medical Biotechnologies, Federico II University of Naples, Naples, Italy; [6]CEINGE - Biotecnologie Avanzate, Naples, Italy and [7]Department of Medicine and Aging Science, "G. d'Annunzio" University of Chieti, Chieti, Italy

Correspondence: L. De Franceschi
lucia.defranceschi@univr.it

Received: August 30, 2022.
Accepted: January 17, 2023.
Early view: January 26, 2023.

https://doi.org/10.3324/haematol.2022.281995

Abstract

Cardiomyopathy deeply affects quality of life and mortality of patients with β-thalassemia or with transfusion-dependent myelodysplastic syndromes. Recently, a link between Nrf2 activity and iron metabolism has been reported in liver iron-overload murine models. Here, we studied C57B6 mice as healthy control and nuclear erythroid factor-2 knockout ($Nrf2^{-/-}$) male mice aged 4 and 12 months. Eleven-month-old wild-type and $Nrf2^{-/-}$ mice were fed with either standard diet or a diet containing 2.5% carbonyl-iron (iron overload [IO]) for 4 weeks. We show that $Nrf2^{-/-}$ mice develop an age-dependent cardiomyopathy, characterized by severe oxidation, degradation of SERCA2A and iron accumulation. This was associated with local hepcidin expression and increased serum non-transferrin-bound iron, which promotes maladaptive cardiac remodeling and interstitial fibrosis related to overactivation of the TGF-β pathway. When mice were exposed to IO diet, the absence of Nrf2 was paradoxically protective against further heart iron accumulation. Indeed, the combination of prolonged oxidation and the burst induced by IO diet resulted in activation of the unfolded protein response (UPR) system, which in turn promotes hepcidin expression independently from heart iron accumulation. In the heart of $Hbb^{th3/+}$ mice, a model of β-thalassemia intermedia, despite the activation of Nrf2 pathway, we found severe protein oxidation, activation of UPR system and cardiac fibrosis independently from heart iron content. We describe the dual role of Nrf2 when aging is combined with IO and its novel interrelation with UPR system to ensure cell survival. We open a new perspective for early and intense treatment of cardiomyopathy in patients with β-thalassemia before the appearance of heart iron accumulation.

Introduction

Cardiomyopathy deeply affects the quality of life and mortality of patients with β-thalassemia or with transfusion-dependent myelodysplastic syndromes.[1-5] Although iron is essential for cardiomyocyte function to sustain aerobic activity, accumulation of iron leads to severe oxidation and cardiomyocyte damage. When iron levels exceed transferrin-binding capacity, the non-transferrin bound iron (NTBI) enters cells and negatively affects the pro-anti-oxidant balance, playing a key role in iron overload (IO) cardiomyopathy. Indeed, studies in patients with β-thalassemia have highlighted the correlation between NTBI and heart disease,[6-8] supporting the important role of oxidative stress catalyzed by Fenton and Haber-Weiss reactions in cardiovascular disease. Iron metabolism is thinning regulated by the hepcidin (Hamp)/ferroportin (Fpn1) axis in close relationship with erythropoiesis.[9] Circulating hepcidin is mainly due to liver production, whereas heart hepcidin expression seems to be more involved in the local effect on heart iron homeostasis. In addition, different factors such as local hypoxia, inflammation, or oxidation may affect heart hepcidin expression independently form iron accumulation.[10-12]

Nuclear erythroid factor-2 (Nrf2) is a fundamental transcription factor involved in redox response. Indeed, Nrf2 modulates the expression of anti-inflammatory and cytoprotective systems important to ensure cell survival in different tissues such as heart, brain, liver, or erythroblasts against oxidation.[13-15] Loss of Nrf2 results in increased susceptibility to cardiovascular diseases induced by angiotensin II or pressure overload or myocardial ischemic reperfusion injury.[16-19] In cardiomyocytes, the biologic relevance of Nrf2 is further supported by the cardiac pro-

tective effects of either Nrf2 inducers or Nrf2 overactivation in different models of cardiovascular disease.[16-19] Recently, a link between Nrf2 activity and iron metabolism has been reported in liver IO throughout the Bmp6 pathway and in β-thalassemic murine erythropoiesis.[20,21] Consistent with this observation, severe oxidative stress such as in doxorubicin-mediated cardiomyopathy, results in overactivation of Nrf2. This upregulates on one hand heme oxygenase-1 (HO-1) expression that degrades heme and increase the pool of intracellular iron and on the other hand anti-oxidant systems such as Gpx to limit oxidative damage.[14,22,23] Despite the growing knowledge on Nrf2 in response to acute oxidative stress in the heart, the role of Nrf2 bridging anti-oxidant systems and iron homeostasis in specialized cells such as cardiomyocytes exposed to prolonged oxidation due to aging or IO is still not understood.

Methods

Animal model and design of the study

C57BL/6J mice as wild-type controls (WT), Nrf2$^{-/-}$ and Hbb$^{th3/+}$ mice on the same background of WT animals were used. Four- and 12-month-old males were studied. Eleven-month-old WT and Nrf2$^{-/-}$ mice were fed with either standard diet (SD) or a diet containing 2.5% carbonyl-iron for 4 weeks.[24] Mice were randomly assigned to the different analysis. Whenever indicated, mice were deeply anesthetized by oxygen and 5% isoflurane and sacrificed by cervical dislocation. Blood and organs were then collected. The Institutional Animal Experimental Committee, University of Verona (CIRSAL) and the Italian Ministry of Health approved the experimental protocol (56DC9.12), following European directive 2010/63/EU and the Federation for Laboratory Animal Science associations guidelines and recommendations.

Echocardiography

Transthoracic echocardiography was performed with a Vevo 2100 echocardiograph (Visual Sonics, Toronto, Canada) equipped with a 22-55 MHz transducer (MicroScan Transducers, MS500D) as previously described.[25]

Heart molecular analysis

Heart iron concentration

Heart iron concentration (HIC) was evaluated in both mouse strains. Details are reported in the *Online Supplementary Appendix*.

Perls' and Masson' trichrome staining

Heart sections were stained with either Perls' or Masson' trichrome stain (N HT15, Sigma-Aldrich) according to the manufacturer's instructions. Images were digitally acquired with an Echo Revolve RVL-100-G microscope. Collagen deposition was quantified by measuring the intensity of red staining on heart sections via Image J software. The cardiomyocyte area was quantified by averaging the area of at least eight cardiomyocytes in a single heart section via Echo Revolve software.

Immunohistochemistry for ferroportin

Heart sections were rehydrated and treated for 10 minutes with 3% H_2O_2 (Sigma Aldrich) to block endogenous peroxidases as previously described.[26] Details are reported in the *Online Supplementary Appendix*.

RNA isolation, cDNA synthesis, and quantitative real-time polymerase chain reaction

Total RNA was extracted from mouse tissues using Trizol reagent (Life Technologies). cDNA synthesis from total RNA (1 μg) was performed using SuperScript II First Strand kits (Life Technologies) as previously described.[27] Details are reported in the *Online Supplementary Appendix*.

Immunoblot analysis

Frozen heart and aorta from each studied group were homogenized and lysed.[28-30] Details are reported in the *Online Supplementary Appendix*.

Heart zymogram for Mmp9 activity and heart caspase 3 activity

Details are reported in the *Online Supplementary Appendix*.[31]

Aorta immuno-microscopic analysis of VCAM-1

Aorta was isolated from WT and Nrf2$^{-/-}$ mice, formalin-fixed and frozen in OCT for immunofluorescence analysis of vCAM1, as previously described. Image acquisition was performed using a Zeiss LSM 510 META confocal microscope.[28] Details are reported in the *Online Supplementary Appendix*.

Non-transferrin bound iron measurement

NTBI measurement was conducted using the ultrafiltration method: 90 μl of serum were incubated with 10 □l of 800 mM nitrilotriacetic acid (NTA) containing 20 μM Fe (pH 7.0) at 23°C for 30 minutes.[26] Details are reported in the *Online Supplementary Appendix*.

Plasma hepcidin measurement

Hepcidin levels were analyzed in mouse plasma using the Hepcidin Murine Compete ELISA kit (Intrinsic Life Sciences, La Jolla, United States), following the manufacturer instructions.[32]

Statistical analysis

Statistical significance of the differences in gene expression were determined using Student's *t*-tests. Stat-

istical significance of multiple comparisons were calculated using ANOVA, *and post* hoc correction was performed using Tukey's multiple comparison tests. A two-sided $P<0.05$ was considered statistically significant.

Results

Nrf2$^{-/-}$ mice develop an age-dependent cardiomyopathy associated with severe oxidation and degradation of SERCA2a

In order to address the question whether Nrf2 might be important to limit the risk of cardiovascular disease related to aging, we studied Nrf2$^{-/-}$ mice at 4 and 12 months of age. Since Erkens *et al.* have previously reported a diastolic dysfunction in 5-6-month-old Nrf2$^{-/-}$ mice,[33] we carried out echocardiography in 12-month-old Nrf2$^{-/-}$ mice compared to WT animals. As shown in Figure 1A, Nrf2$^{-/-}$ mice showed diastolic dysfunction as reversible restrictive filling pattern grade 3, characterized by reduced MV deceleration time, which was associated with increased E/A and left ventricular dysfunction. This is consistent with hypertrophic cardiac ultrasound pattern as also supported by increased in heart-to-body-weight ratio (*Online Supplementary Figure S1A*) and the upregulation of atrial natriuretic peptide (ANP), a marker of cardiac remodeling and hypertrophy, in the heart of Nrf2$^{-/-}$ mice when compared to WT animals (Figure 1B).[34,35] Noteworthy, increased cell volume of cardiomyocytes was found in the heart of 12-months-old Nrf2$^{-/-}$ mice, suggesting an attempt to compensate for loss of cardiomyocyte function/damage in aged Nrf2$^{-/-}$ mice (*Online Supplementary Figure S1B*). The absence of Nrf2 resulted in increased heart protein oxidations related to downregulation of Nrf2-dependent cytoprotective systems important in cardiomyocyte homeostasis such as catalase, SOD1 or Nqo1 (Figure 1C, D; *Online Supplementary Figure S1C, D*). In the heart of Nrf2$^{-/-}$ mice, we also observed degradation of the sarcoplasmic reticulum calcium ATPase cardiac isoform 2 (SERCA2a), a calcium transport system important for myocardial performance, in agreement with the severe and sustained oxidation observed in mice genetically lacking Nfe2l2 (Figure 1E; SERCA2A proteolytic residues between 60-75 kDa; *Online Supplementary Figure S1E*).[31, 36-39] Consistent with the degradation of SERCA2a protein, we found a compensatory upregulation of sodium calcium exchanger protein 1 (Ncx1) expression as reported in other models of cardiomyopathies (*Online Supplementary Figure S1F*).[40,41] SERCA2A is degraded by metalloproteinase (Mmps) that participates in myocardial remodeling as collagenase.[31,37,42,43] Here, we found increased expression and activity of Mmp9 Nrf2$^{-/-}$ mice when compared with WT animals (Figure 1F; *Online Supplementary Figure S2A*). No major change in Mmp2 activity was observed. In addition, we found increased caspase 3 activity, a key molecular marker of apoptosis in the heart of Nrf2$^{-/-}$ mice when compared to WT animals (Figure 1G). This was associated with age-dependent accumulation of K48 polyubiquitin proteins, a key linkage signal for degradation of dysfunctional proteins[44-47] (*Online Supplementary Figure S2B*). Indeed, upregulation of *necrostatin-1* mRNA expression observed in the heart form Nrf2$^{-/-}$ mice might be an attempt to control loss of cardiomyocytes induced by chronic oxidation in the absence of Nrf2 (*Online Supplementary Figure S2C*). Taken together, our data indicate that Nrf2$^{-/-}$ mice develop an age-dependent cardiomyopathy characterized by severe and sustained oxidation, resulting in activation of myocardial remodeling and pro-apoptotic pathways.

Loss of Nrf2 is associated with chronic cardiac inflammation and vascular dysfunction

The activation of Mmp9 led us to evaluate whether the absence of Nrf2 might favor the activation of NF-kB p65, a redox- and inflammatory-related transcription factor, as a back-up mechanism to limit cardiomyocyte damage. In the heart of Nrf2$^{-/-}$ mice, we found activation of NF-kB p65 when compared to WT animals (Figure 2A; *Online Supplementary Figure S2D*). This was associated with upregulation of Il-1b expression in both 4- and 12-month-old Nrf2$^{-/-}$ mice; whereas Il-6 expression was increased only iin the heart of 4-months-old Nrf2$^{-/-}$ mice when compared to WT animals (*Online Supplementary Figure S2SE*). In Nrf2$^{-/-}$ mice, chronic cardiac inflammation was further supported by upregulation of endothelin-1 (ET-1) expression, a potent pro-inflammatory and vasoactive cytokine as well as of ICAM-1 and VCAM-1, known markers of inflammatory vasculopathy (Figure 2B; *Online Supplementary Figure S2F*). Similar data were also observed in isolated aorta of Nrf2$^{-/-}$ mice, indicating the presence of both local and systemic vascular dysfunction in the absence of Nrf2 (*Online Supplementary Figure S3A*). Collectively, our data indicate that maladaptive inflammation characterizes the heart of Nrf2$^{-/-}$ mice, contributing to reduced cardiomyocyte performance and promoting cardiac remodeling.

Heart iron accumulation characterizes cardiomyopathy of Nrf2$^{-/-}$ mice, leading to cardiac fibrosis

Since previous studies have linked Nrf2 function and iron homeostasis, we asked whether iron accumulated in the heart of Nrf2$^{-/-}$ mice could trigger oxidative stress and inflammatory response. As shown in Figure 2C, we found increased iron deposits in the heart of Nrf2$^{-/-}$ mice when compared to WT animals. This is in agreement with increased NTBI that contributes to formation of ROS (Figure 2D). In Nrf2$^{-/-}$ mice, heart expression of Hamp was significantly lower than in WT animals (Figure 2E). Noteworthy, we observed higher heart expression of *Bmp2* mRNA in both young and old Nrf2$^{-/-}$ mice than in WT animals (*On-*

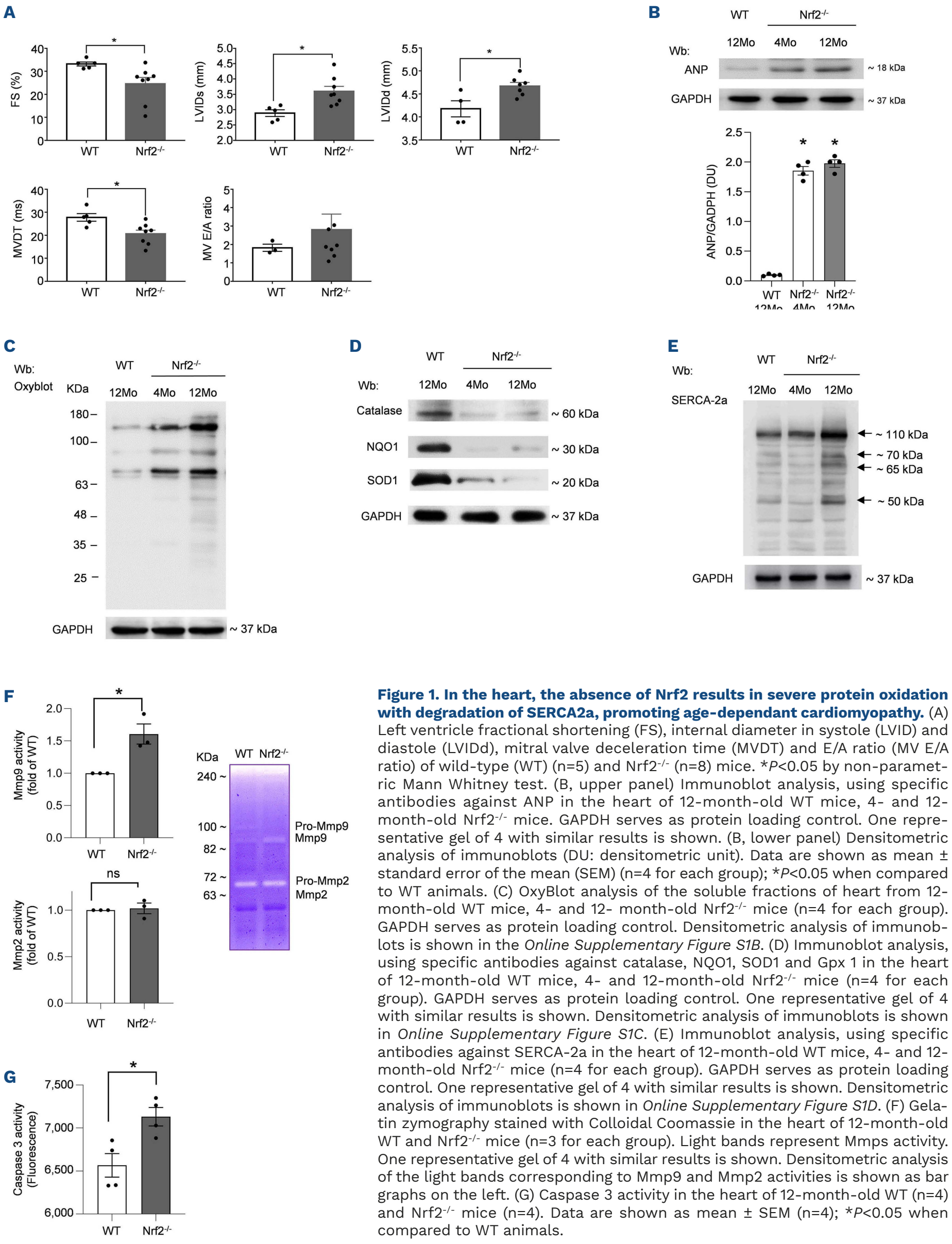

Figure 1. In the heart, the absence of Nrf2 results in severe protein oxidation with degradation of SERCA2a, promoting age-dependant cardiomyopathy. (A) Left ventricle fractional shortening (FS), internal diameter in systole (LVID) and diastole (LVIDd), mitral valve deceleration time (MVDT) and E/A ratio (MV E/A ratio) of wild-type (WT) (n=5) and Nrf2$^{-/-}$ (n=8) mice. *P<0.05 by non-parametric Mann Whitney test. (B, upper panel) Immunoblot analysis, using specific antibodies against ANP in the heart of 12-month-old WT mice, 4- and 12-month-old Nrf2$^{-/-}$ mice. GAPDH serves as protein loading control. One representative gel of 4 with similar results is shown. (B, lower panel) Densitometric analysis of immunoblots (DU: densitometric unit). Data are shown as mean ± standard error of the mean (SEM) (n=4 for each group); *P<0.05 when compared to WT animals. (C) OxyBlot analysis of the soluble fractions of heart from 12-month-old WT mice, 4- and 12- month-old Nrf2$^{-/-}$ mice (n=4 for each group). GAPDH serves as protein loading control. Densitometric analysis of immunoblots is shown in the *Online Supplementary Figure S1B*. (D) Immunoblot analysis, using specific antibodies against catalase, NQO1, SOD1 and Gpx 1 in the heart of 12-month-old WT mice, 4- and 12-month-old Nrf2$^{-/-}$ mice (n=4 for each group). GAPDH serves as protein loading control. One representative gel of 4 with similar results is shown. Densitometric analysis of immunoblots is shown in *Online Supplementary Figure S1C*. (E) Immunoblot analysis, using specific antibodies against SERCA-2a in the heart of 12-month-old WT mice, 4- and 12-month-old Nrf2$^{-/-}$ mice (n=4 for each group). GAPDH serves as protein loading control. One representative gel of 4 with similar results is shown. Densitometric analysis of immunoblots is shown in *Online Supplementary Figure S1D*. (F) Gelatin zymography stained with Colloidal Coomassie in the heart of 12-month-old WT and Nrf2$^{-/-}$ mice (n=3 for each group). Light bands represent Mmps activity. One representative gel of 4 with similar results is shown. Densitometric analysis of the light bands corresponding to Mmp9 and Mmp2 activities is shown as bar graphs on the left. (G) Caspase 3 activity in the heart of 12-month-old WT (n=4) and Nrf2$^{-/-}$ mice (n=4). Data are shown as mean ± SEM (n=4); *P<0.05 when compared to WT animals.

line Supplementary Figure S3B). This might be part of compensatory mechanisms antagonizing prohypertrophic and pro-apoptotic stimuli such as chronic cardiac oxidation and inflammation.[48] Plasma hepcidin was similar in both mouse strains (*Online Supplementary Figure S3C*). Reduced heart expression of Hamp and of Hamp/HIC ratio were associated with accumulation of Fpn1 in the heart of Nrf2$^{-/-}$ mice compared to WT animals (Figure 2F; *Online Supplementary Figure S3D*). This agrees with Fpn1 post-translational regulation by Hamp as previously observed

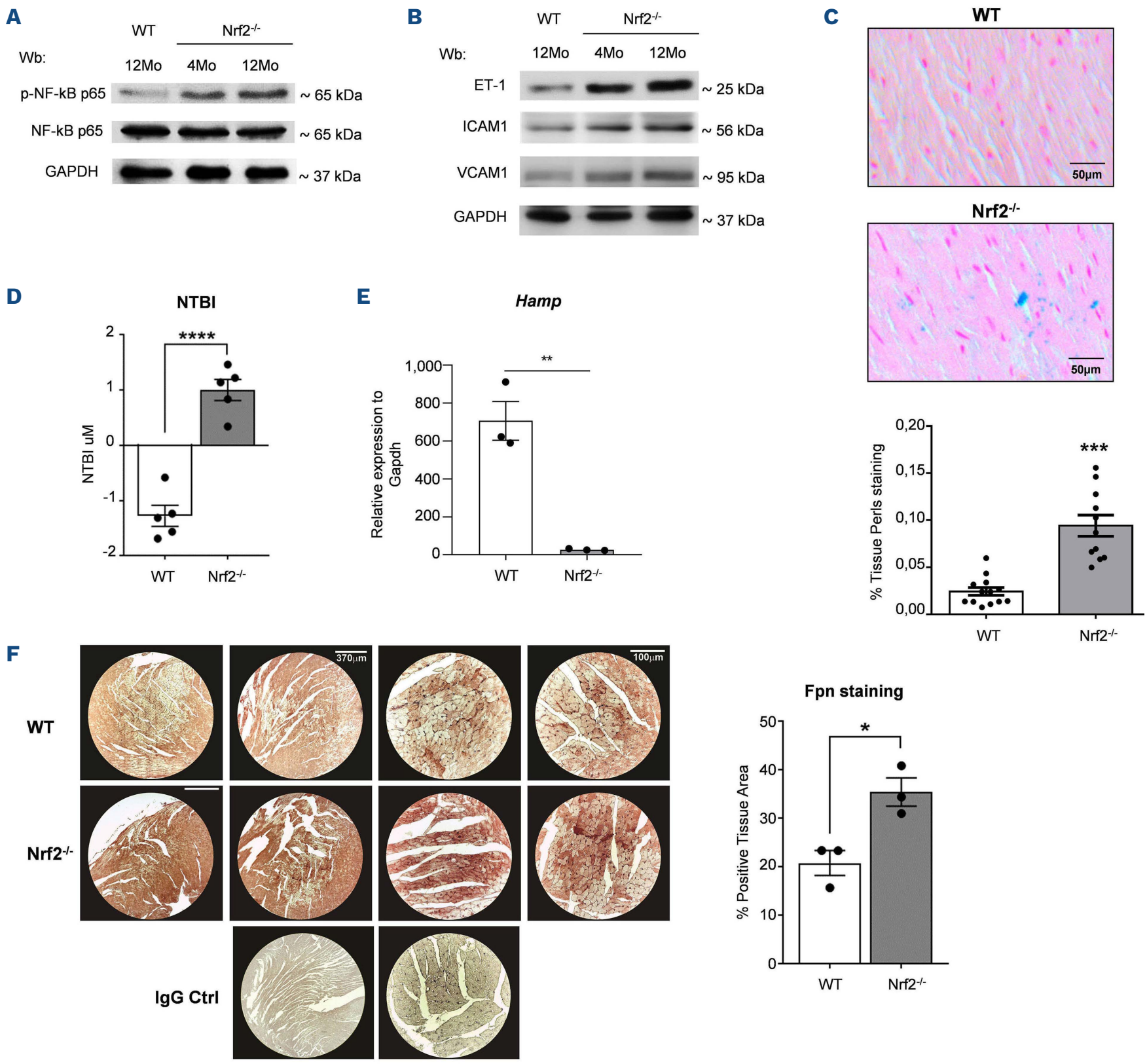

Figure 2. In the heart, Nrf2$^{-/-}$ mice display iron accumulation and redox related activation of activation of NF-kB p65, sustaining inflammatory vasculopathy. (A) Immunoblot analysis, using specific antibodies against phosphorylated (p)NF-κB p65, NF-κB p65 in the heart of 12-month-old wild-type (WT) mice, 4- and 12-month-old Nrf2$^{-/-}$ mice (n=4 for each group). GAPDH serves as protein loading control. One representative gel of 4 with similar results is shown. Densitometric analysis of immunoblots is shown in *Online Supplementary Figure S2D*. (B) Immunoblot analysis, using specific antibodies against ET-1, ICAM1 and VCAM1 in the heart of 12-month-old WT mice, 4- and 12-month-old Nrf2$^{-/-}$ mice (n=4 for each group). GAPDH serves as protein loading control. One representative gel of 4 with similar results is shown. Densitometric analysis of immunoblots is shown in *Online Supplementary Figure S1F*. (C) Perl's staining in heart tissue sections of Nrf2$^{-/-}$ and WT mice. A representative picture is shown. The quantification of the % of stained tissue is shown on the right. (D) Non-trasferrin-bound iron (NTBI) measurement in the serum of WT and Nrf2$^{-/-}$ mice (n=5 for each group). (E) Quantification of *Hamp* mRNA levels normalized to Gapdh in the heart of WT and Nrf2$^{-/-}$ mice (n=3 for each group). Data are means ± standard deviation of 3 experiments (**P<0.001, Student's t-test). (F) Representative images of FPN immunostaining on heart sections of WT and Nrf2$^{-/-}$ mice (scale bars: 370/100 μm) and relative quantification expressed as percentage positive tissue area (n=3 for each group).

by Aschemeyer *et al.*[49] Taken together these data support the synergic effect of iron accumulation and defective antioxidant systems in the development of age-dependent cardiomyopathy in Nrf2$^{-/-}$ mice.

Since Nrf2 has been reported to prevent maladaptive cardiac remodeling and interstitial fibrosis,[50,51] we evaluated collagen deposition in the heart of Nrf2$^{-/-}$ mice. As shown in Figure 3A, collagen deposition was significantly higher in the heart of Nrf2$^{-/-}$ mice than in WT animals. This was associated with activation of TGF-β1 receptor, which plays a crucial role in profibrotic pathway(s) and in extracellular matrix accumulation (Figure 3B).[52,53] In addition, we found increased expression of platelet-derived growth factor-B (PDGF-B) and activation of its receptor (PDGFR-B) as well as of fibroblast growth factor receptor (FGF-R), which are all involved in matrix remodeling and profibrotic events in collaboration with TGF-β1 system (Figure 3B).[54,55] Collectively our data indicate that the absence of Nrf2 leads to age-dependent cardiomyopathy characterized by chronic oxidation amplified by iron accumulation due to abnormal local iron homeostasis. This results in cardiac inflammation and fibrosis in Nrf2$^{-/-}$ mice.

Nrf2$^{-/-}$ mice exposed to iron overload develop compensatory cardiac hypertrophy independently from iron accumulation

Since Lim *et al.* have previously reported liver iron accumulation in Nrf2$^{-/-}$ mice exposed to iron overload diet due to the perturbation of Hamp-Bmp6 pathway, 11-month-old Nrf2$^{-/-}$ mice were fed with either SD or IO diet containing 2.5% carbonyl-iron for 4 weeks. In WT animals, we observed in Nrf2 activation in the heart when compared

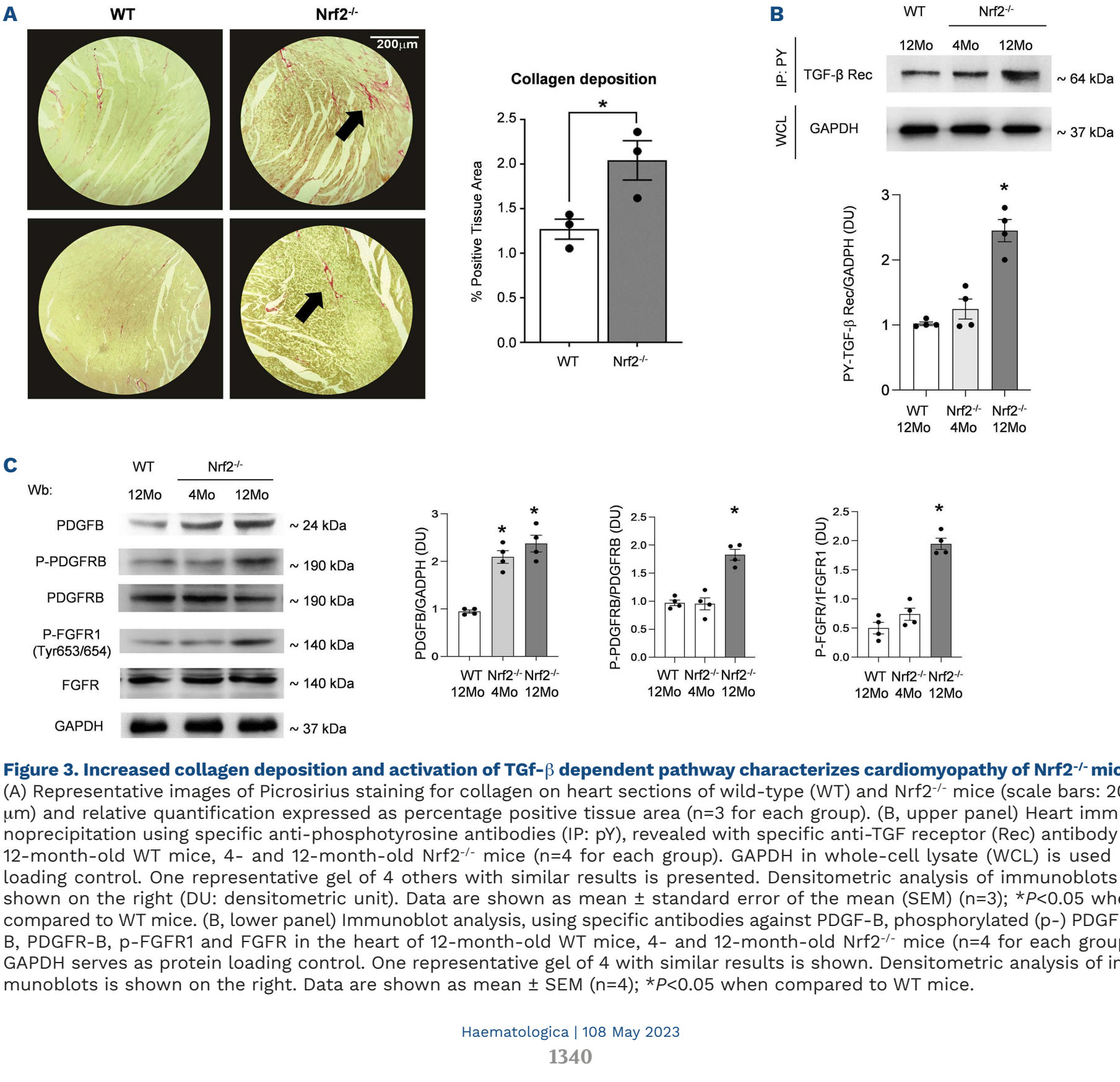

Figure 3. Increased collagen deposition and activation of TGf-β dependent pathway characterizes cardiomyopathy of Nrf2$^{-/-}$ mice. (A) Representative images of Picrosirius staining for collagen on heart sections of wild-type (WT) and Nrf2$^{-/-}$ mice (scale bars: 200 μm) and relative quantification expressed as percentage positive tissue area (n=3 for each group). (B, upper panel) Heart immunoprecipitation using specific anti-phosphotyrosine antibodies (IP: pY), revealed with specific anti-TGF receptor (Rec) antibody in 12-month-old WT mice, 4- and 12-month-old Nrf2$^{-/-}$ mice (n=4 for each group). GAPDH in whole-cell lysate (WCL) is used as loading control. One representative gel of 4 others with similar results is presented. Densitometric analysis of immunoblots is shown on the right (DU: densitometric unit). Data are shown as mean ± standard error of the mean (SEM) (n=3); *P<0.05 when compared to WT mice. (B, lower panel) Immunoblot analysis, using specific antibodies against PDGF-B, phosphorylated (p-) PDGFR-B, PDGFR-B, p-FGFR1 and FGFR in the heart of 12-month-old WT mice, 4- and 12-month-old Nrf2$^{-/-}$ mice (n=4 for each group). GAPDH serves as protein loading control. One representative gel of 4 with similar results is shown. Densitometric analysis of immunoblots is shown on the right. Data are shown as mean ± SEM (n=4); *P<0.05 when compared to WT mice.

to standard diet animals (*Online Supplementary Figure S4A*). This was in parallel with a better survival rate compared to Nrf2$^{-/-}$ mice (*Online Supplementary Figure S4B*).
Nrf2$^{-/-}$ mice developed cardiac hypertrophy in response to IO compared to WT animals (Figure 4A; *Online Supplementary Figure S4C*). This was associated with a further increase of cardiomyocyte area, compensatory to myocyte loss in IO Nrf2$^{-/-}$ mice (Figure 4B). In agreement, cardiac *troponin T* gene expression was increased in IO Nrf2$^{-/-}$ mice compared to IO WT animals (*Online Supplementary Figure S4D*). Perls' staining revealed heart iron accumulation in WT animals, which was higher than in the heart of Nrf2-/- mice exposed to IO (*Online Supplementary Figure S5A*). In agreement with previous report by Lim *et a*l., liver iron accumulation was more severe in Nrf2$^{-/-}$ mice than in WT animals and Hamp and Bmp6 expression was downregulated (*Online Supplementary Figure S5B, C*). NTBI levels were almost unaffected by IO in Nrf2$^{-/-}$ mice, while NTBI significantly increased in IO WT mice compared to standard diet WT animals (*Online Supplementary Figure S6A*). Heart *Hamp* mRNA expression was higher in IO Nrf2$^{-/-}$ mice than in IO WT animals (Figure 4C). Activation of both NF-kBp65 and STAT3 in response to IO was observed only in the heart of WT animals (*Online Supplementary Figure S6B*). In agreement, we found upregulation of heart *Il-1b* and *Il-6* mRNA expression only in the heart of WT animals and not in IO Nrf2$^{-/-}$ mice (*Online Supplementary Figure S6C*). Noteworthy, *Bmp2* and *Bmp6* mRNA expression was similar in both mouse strains exposed to IO (*Online Supplementary Figure S6D*). Previous reports have highlighted the link between proteostasis, upregulation of UPR system in response to endoplasmic reticulum (ER)-stress and hepcidin expression.[38,56] As shown in Figure 4E and *Online Supplementary Figure S6E*, IO resulted in accumulation of K48 polyubiquitin proteins in the heart from WT animals compared to SD-treated animals, whereas no change in the degree of K48 polyubiquitin protein accumulation was observed in Nrf2$^{-/-}$ mice under IO diet *versus* SD. We then sought to investigate the UPR system focusing on the ATF6 branch based on previous reports on diabetic cardiomyopathy.[38,57,58] We found increased expression of ATF6, as well as related GADD34 and CHOP in the heart of IO Nrf2$^{-/-}$ mice when compared to either SD treated Nrf2$^{-/-}$ mice or IO WT animals (Figure 4F; *Online Supplementary Figure S6F*). This was associated with the increase of apoptotic markers beside CHOP such as caspase-3 determined as both pro-caspase 3/caspase 3 ratio and caspase 3 activity in the heart of IO Nrf2$^{-/-}$ mice when compared to IO WT animals (*Online Supplementary Figure S7A*). Heart expression of necrostatin-1 in the heart was significantly lower in IO Nrf2$^{-/-}$ mice than in IO WT animals, suggesting an exhaustion of cardiomyocyte defense mechanism towards a pro-apoptotic phenotype (*Online Supplementary Figure S7B*).
In addition, we observed a further increase of PDGF-B expression when compared to standard diet Nrf2$^{-/-}$ animals (*Online Supplementary Figure S7C*), suggesting a worsening of extracellular matrix remodeling in response to IO. Collagen deposition show a trend of further increase in IO Nrf2$^{-/-}$ mice compared to IO WT animals (Figure 4D; *Online Supplementary Figure S7D*). This is of interest since ER stress and activation of UPR pathways have been linked to fibrotic organ remodeling.[59,60] No major change in heart Fpn1 staining was observed in IO Nrf2$^{-/-}$ mice compared IO WT mice (*Online Supplementary Figure S7E*).
In order to understand the impact of IO on vascular system in Nrf2$^{-/-}$ mice, we evaluated the effect of IO on isolated aorta of both mouse strains. We found further upregulation of VCAM-1, as marker of inflammatory vasculopathy in IO Nrf2$^{-/-}$ mice when compared to IO WT animals (Figure 4G; *Online Supplementary Figure S8*). IO induced increased expression of ICAM-1 in isolated aorta of WT mice compared to aorta from standard diet animals (*Online Supplementary Figure S8*).
Taken together these data indicate that in IO Nrf2$^{-/-}$ mice the upregulation of Hamp is independent from Bmp6 expression, but related to prolonged unmitigated ER stress, highlighting the peculiarity of the heart *versus* liver setting.[20] Thus, the absence of Nrf2 promotes cardiac hypertrophy as an attempt to compensate cardiomyocyte death in the presence of progressive exhaustion of adaptive mechanisms against chronic oxidation.

Chronic cardiac oxidation and inflammation leads to age-dependent hypertrophic cardiomyopathy in murine β-thalassemia

Hypertrophic cardiomyopathy is a severe invalidating complication of patients with β-thalassemia.[4,61,62] Recent studies in patients with β-thalassemia have shown that left ventricular diastolic dysfunction might appear early in the absence of magnetic resonance iron heart accumulation, suggesting a biocomplexity of the pathogenesis of cardiomyopathy in β-thalassemia happening behind the heart accumulation of iron.[4,61] As shown in Figure 5A, 12-month-old β-thalassemic (Hbb$^{th3/+}$) mice develop a left ventricle hypertrophy, associated with increased cardiomyocyte areas (Figure 5B) and heart expression of atrial natriuretic peptide (ANP) (*Online Supplementary Figure S9A*). This together with increased caspase 3 activity in the heart support the reduction of cardiomyocyte performance associated with cardiomyocyte death in Hbb$^{th3/+}$ when compared to WT animals (*Online Supplementary Figure S9B*). Although heart iron levels by Perls' staining were similar in Hbb$^{th3/+}$ and WT animals, NTBI was significantly higher in Hbb$^{th3/+}$ than in WT mice (Figure 5C; *Online Supplementary Figure S9C*). Heart Hamp expression was significantly reduced in Hbb$^{th3/+}$ mice compared to WT animals (*Online Supplementary Figure S10A*). Noteworthy,

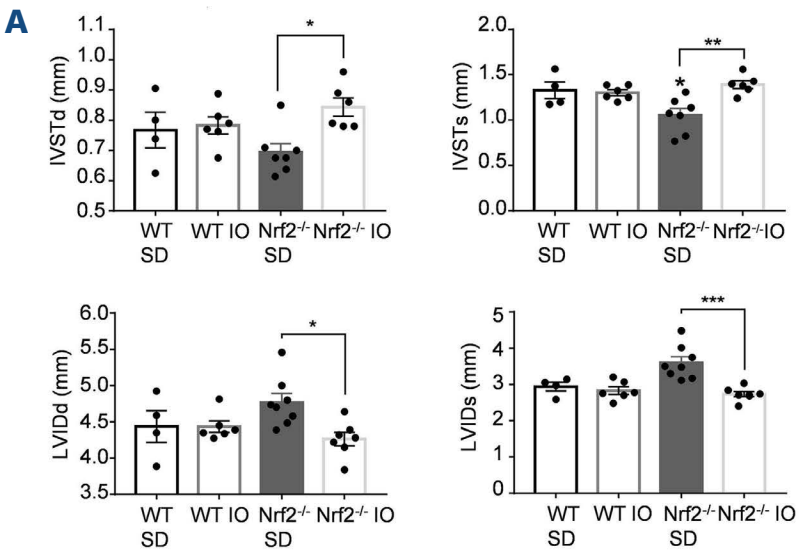

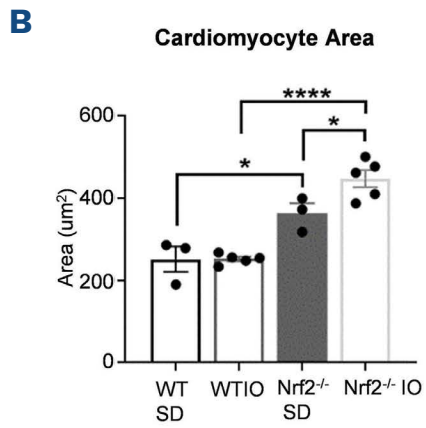

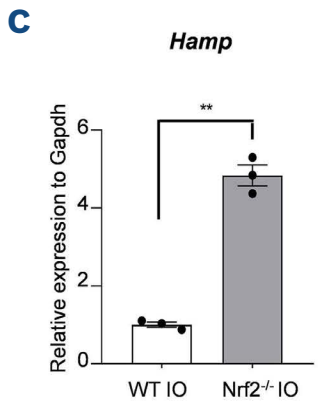

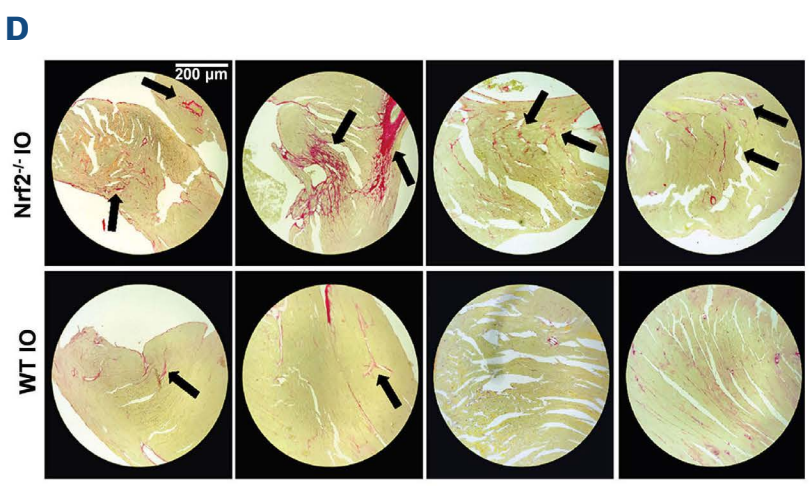

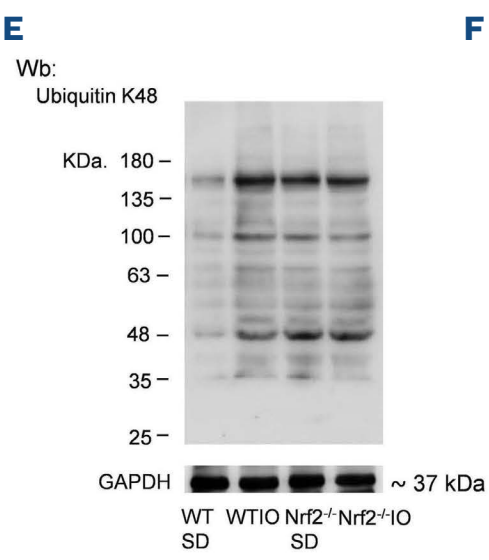

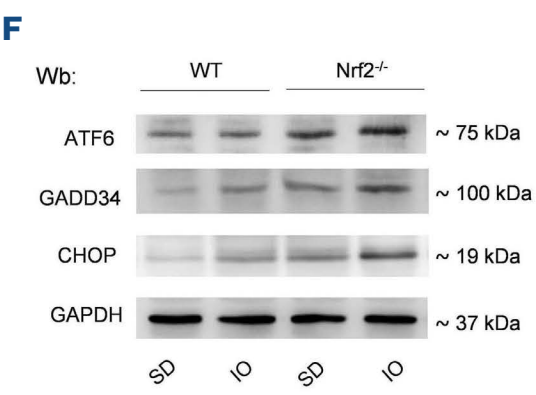

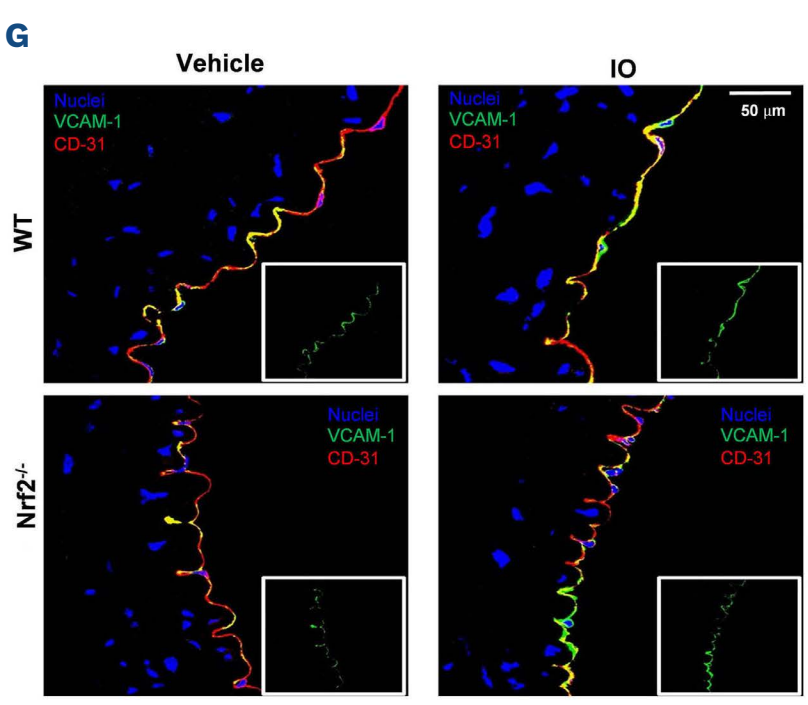

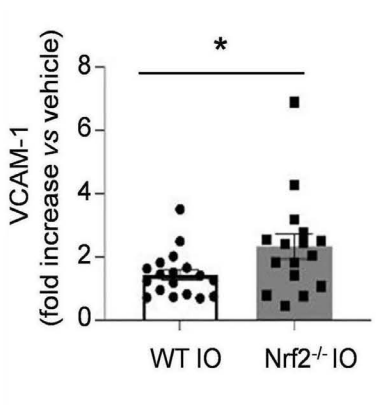

Figure 4. Nrf2$^{-/-}$ mice exposed to iron overload develop compensatory cardiac hypertrophy associated with activation of unfolded protein response system, resulting in upregulation of hepcidin expression independently from iron heart accumulation. (A) Interventricular septum thickness and left ventricle internal diameter in diastole (IVSTd and LVIDd, respectively) and systole (IVST and LVIDs, respectively) of untreated and iron-overloaded (IO) wild-type (WT) and Nrf2$^{-/-}$ mice. WT: n=4; WT IO: n=6; Nrf2$^{-/-}$: n=8; Nrf2$^{-/-}$ IO: n= 7. WT *vs* Nrf2$^{-/-}$: **P*<0.05 and ***P*<0.01; IO *vs*. untreated within each group: $^{\#}$*P*<0.05, $^{\#\#}$*P*<0.01 and $^{\#\#\#}$*P*<0.001, by one-way ANOVA. (B) Quantification of the average cardiomyocyte area in WT and Nrf2-/- mice exposed to standard diet (SD) or IO diet (IO: 2.5% carbonyl-iron for 4 weeks). (C) Quantification of *Hamp* mRNA levels normalized to Gapdh in the heart of WT IO and Nrf2$^{-/-}$ IO mice (n=3 for each group). Data are means ± standard deviation of experiments (***P*<0.001, Student's *t*-test). (D) Representative images of Picrosirius staining for collagen on heart sections of WT and Nrf2$^{-/-}$ mice (scale bars: 370 µm) exposed to IO diet (IO: 2.5% carbonyl-iron for 4 weeks). (E) Western blot (Wb) analysis of ubiquitinated proteins (K48) in the heart of WT and Nrf2$^{-/-}$ mice exposed to SD or IO diet (IO: 2.5% carbonyl-iron for 4 weeks) (n=4 for each group). GAPDH is the protein loading control. Quantification of band area was performed by densitometry and is shown in *Online Supplementary Figure S6E*. (F) Immunoblot analysis, using specific antibodies against ATF6, GADD34 and CHOP in the heart of WT and Nrf2$^{-/-}$ mice exposed to SD or IO diet (IO: 2.5% carbonyl-iron for 4 weeks) (n=4 for each group). GAPDH serves as protein loading control. One representative gel from 4 with similar results is shown. Densitometric analysis of immunoblots is shown in *Online Supplementary Figure S6F*. (G) VCAM-1 expression evaluated as fluorescence intensity (green channel) in aortas isolated from WT and Nrf2$^{-/-}$ mice exposed to SD or IO diet (IO: 2.5% carbonyl-iron for 4 weeks) (n=3 for each group). Semi-quantitative analysis of the number of pixels in the selected fields is shown in the bar graph as fold-increase compared to SD treated animals (right panel), **P*<0.05 compared to WT animals.

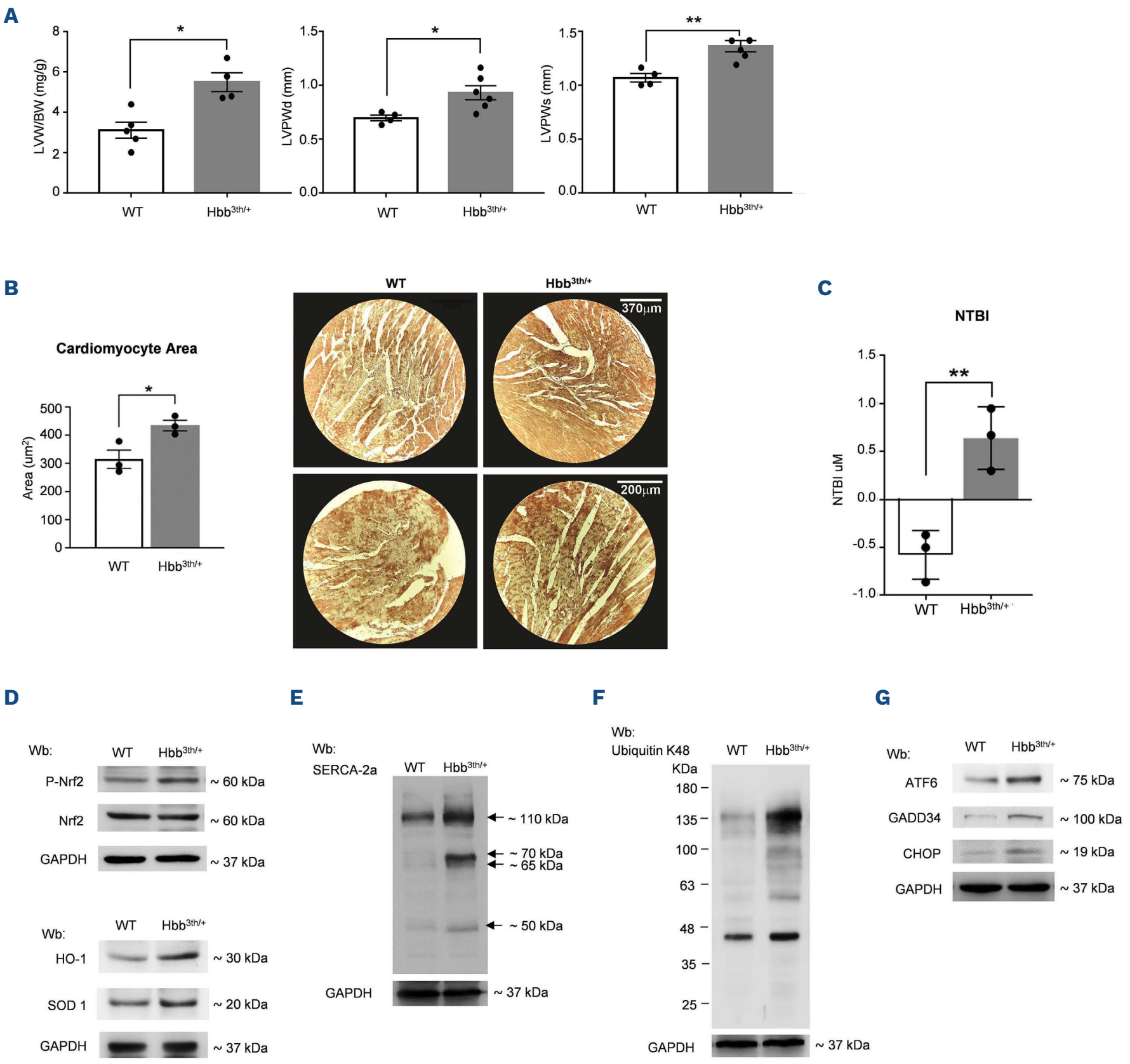

Figure 5. In murine β-thalassemia, cardiomyopathy is related to severe oxidation, overwhelming cytoprotective mechanisms with degradation of SERCA2A and accumulation of polyubiquinated proteins independently from heart iron accumulation. (A) Left ventricle weight/body weight ratio (LVW/BW) and left ventricle posterior wall thickness in diastole (LVPWTd) and systole (LVPWTs) of 12-month-old wild-type (WT) (n=4) and Hbb$^{th3/+}$, a model of β-thalassemia (n=6) mice. *P<0.05 and **P<0.01 by non-parametric Mann Whitney test. (B) Quantification of the average cardiomyocyte area in WT and Hbb$^{th3/+}$ mice (n=3 for each group); representative images of FPN immunostaining on heart sections of WT and Hbb$^{th3/+}$ mice (scale bars: 370/200 µm). (C) Non-transferrin bound iron (NTBI) measurement in the serum of WT and Hbb$^{th3/+}$ mice (n=3 for each group). (D, upper panel) Immunoblot analysis, using specific antibodies against phosphorylated p-Nrf2, and Nrf2, in the heart of 12-month-old WT and Hbb$^{th3/+}$ mice (n=4 for each group). GAPDH serves as protein loading control. One representative gel of 3 with similar results is shown. Densitometric analysis of immunoblots is shown in *Online Supplementary Figure S10C*. (D, lower panel) Immunoblot analysis, using specific antibodies against HO-1 and SOD 1 in the heart of 12-month-old WT and Hbb$^{th3/+}$ mice (n=4 for each group). GAPDH serves as protein loading control. One representative gel of 3 with similar results is shown. Densitometric analysis of immunoblots is shown in *Online Supplementary Figure S10C*. (E) Immunoblot analysis, using specific antibodies against SERCA-2a in the heart of 12-months-old WT and Hbbth3/+ mice (n=4 for each group). GAPDH serves as protein loading control. One representative gel of 3 with similar results is shown. Densitometric analysis of immunoblots is shown in *Online Supplementary Figure S10D*. (F) Western blot (Wb) analysis of ubiquitinated proteins (K48) in the heart of 12-month-old WT and Hbb$^{th3/+}$ mice (n=4 for each group). GAPDH is the protein loading control. Quantification of band area was performed by densitometry and is shown in *Online Supplementary Figure S10E*. (G) Immunoblot analysis, using specific antibodies against ATF6, GADD34 and CHOP in the heart of 12-month-old WT and Hbb$^{th3/+}$ mice (n=4 for each group). GAPDH serves as protein loading control. One representative gel of 3 with similar results is shown. Densitometric analysis of immunoblots is shown in *Online Supplementary Figure S10F*.

Bmp6 expression was significantly higher in the heart of Hbb$^{th3/+}$ mice than in WT animals (*Online Supplementary Figure S10A*). No major change in the heart Bmp2 expression was observed between the two mouse strains (*Online Supplementary Figure S10A*). This agrees with Bmp6 participating in compensatory mechanisms against severe oxidation and stimulating cardiomyocyte hypertrophy more than in iron homeostasis.[63] Indeed, heart protein oxidation was increased in Hbb$^{th3/+}$ when compared to WT animals (*Online Supplementary Figure S10B*). This is in agreement with activation of Nrf2^{-} and Nrf2^{-}related cytoprotective systems such as HO-1 and SOD-1 in the heart of Hbb$^{th3/+}$ mice compared to WT animals (Figure 5D; *Online Supplementary Figure S10C*). In addition, in the heart of Hbb$^{th3/+}$ mice, chronic oxidation promoted (i) degradation of SERCA2a (Figure 5E; *Online Supplementary Figure S10D*); and accumulation of K48 polyubiquitin proteins (Figure 5F; *Online Supplementary Figure S11A*); and upregulation of ATF6 (Figure 5G; *Online Supplementary Figure S11B*), resulting in increased expression of pro-apoptotic protein GADD34 (Figure 5G; *Online Supplementary Figure S11G*). The synergic effect of chronic cardiac oxidation, activation of the UPR system and inflammation promoted (i) activation of TGF-β receptor (Figure 6A; *Online Supplementary Figure S11C*); (ii) increase expression of PDGF-B and activation of PDGF-receptor and FGF-receptor (Figure 6B; *Online Supplementary Figure S11D*), ending in heart collagen deposition in Hbb$^{th3/+}$ mice (Figure 6C). Collectively, our data indicate that β-thalassemic-related cardiomyopathy is promoted by the combination of different factors having oxidation as an early and central event in diastolic dysfunction and cardiac fibrosis that might be worsened by cardiac iron accumulation as observed in patients with β-thalassemia.

Discussion

Here, we show the dual effect of Nrf2 in cardiomyopathy related to sustained and prolonged oxidation as observed in aging or in iron overload models.

We show that mice genetically lacking *Nfe2l2* are highly sensitive to age-induced oxidation, which is associated with heart iron accumulation. In aged Nrf2$^{-/-}$ mice, the downregulation of cardiac hepcidin expression agrees with the lower expression of Bmp6 compared to WT animals. In old Nrf2$^{-/-}$ mice, the detrimental effect of prolonged oxidative stress leads to maladaptive response, resulting in reduced cardiomyocyte performance, degradation of the key cell Ca^{2+} modulator, SERCA2a, and accumulation of K48 polyubiquitinated proteins.[64] The proteotoxic stress promotes cardiac fibrosis throughout the activation of the TGF-β1 pathway. This highlights the key role of Nrf2 function against age-related cardiomyopathy and gives further importance to the cumulative effects of pro-oxidant factors such as age, diabetes or inflammatory vasculopathy on the pathogenesis of hypertrophic cardiomyopathy.[65,66]

When IO was used as additional stress to aging, the absence of Nrf2 resulted in cardiac hypertrophy as an attempt to compensate for the loss of cardiomyocytes linked to the detrimental effect of accumulation of K48 polyubiquitinated proteins. This disrupts ER homeostasis, resulting in ER stress and leading to the activation of the UPR system. Whenever the stress is sustained or prolonged, the activation of UPR might not be sufficient to limit/resolve the stress, ending in activation of the pro-apoptotic pathway.[59,67] Among the three branches of the UPR system, the ATF6/CHOP and the CHOP-activating GADD34 pathways have been described to play a crucial role in ischemic/reperfusion myocardial injury or in cardiac hypertrophy or in heart disease related to diabetes.[38,59,67] Indeed, we found overactivation of ATF in IO Nrf2$^{-/-}$ mice but not in IO WT animals,[57,68] resulting in upregulation of CHOP which in turn induces the expression of DNA damage-inducible proteins such as GADD34. These factors collectively sustain pro-apoptotic pathways such as caspase 3 signaling. As part of the ER stress response, we observed local upregulation of hepcidin, which protects the heart of further iron accumulation. This conclusion is supported by a previous report linking Hamp expression to ER stress and the activation of UPR system.[56] Indeed, in Nrf2$^{-/-}$ mice exposed to IO, we found increased Hamp expression independently from Bmp2-6, whose expression is similar to that observed in IO WT animals.

Since cardiomyopathy negatively impacts the quality of life of patients with transfusion-dependent and transfusion-independent β-thalassemia, we evaluated cardiomyopathy in aged Hbb$^{th3/+}$ mice. Although we did not find significant heart iron accumulation, we observed increased NTBI and severe cardiac protein oxidation, which was associated with activation of Nrf2 and upregulation of related antioxidant and cytoprotective systems. In Hbb$^{th3/+}$ mice, the prolonged cardiac oxidation resulted in increased expression as well as degradation of SERCA2a. This might contribute to impaired myocardial relaxation associated with left ventricular hypertrophy in Hbb$^{th3/+}$ mice.[33] Noteworthy, upregulation of ATF6 in response to ER stress might contribute to upregulation of SERCA2a observed in the heart of Hbb$^{th3/+}$ mice as an adaptive mechanism against the impairment of cardiomyocyte performance. In Hbb$^{th3/+}$ mice, the unbalance between prolonged oxidation and cytoprotective systems even in the absence of heart iron accumulation is associated with cardiomyopathy characterized by proteotoxic stress and activation of the UPR system.[55] This latter has been described to contribute to the activation of the TGF-β1 pro-fibrotic pathway in lung fibrosis.[69,70] Here, we found the activation of the TGF-β1 system associated with collagen

deposition in the heart of both Nrf2$^{-/-}$ and Hbb$^{th3/+}$ mice. In the setting of patients with transfusion-dependent or -independent β-thalassemia even in the absence of cardiac iron deposition, early treatment with agents used in the management of heart failure characterized by SERCA2a dysfunction such as β-blockers, ACE-inhibitors and aldosterone antagonists are beneficial.

In conclusion, our data highlight the dual role of Nrf2 as redox-related transcriptional factor, which is also interrelated with the UPR system to ensure cell survival. The

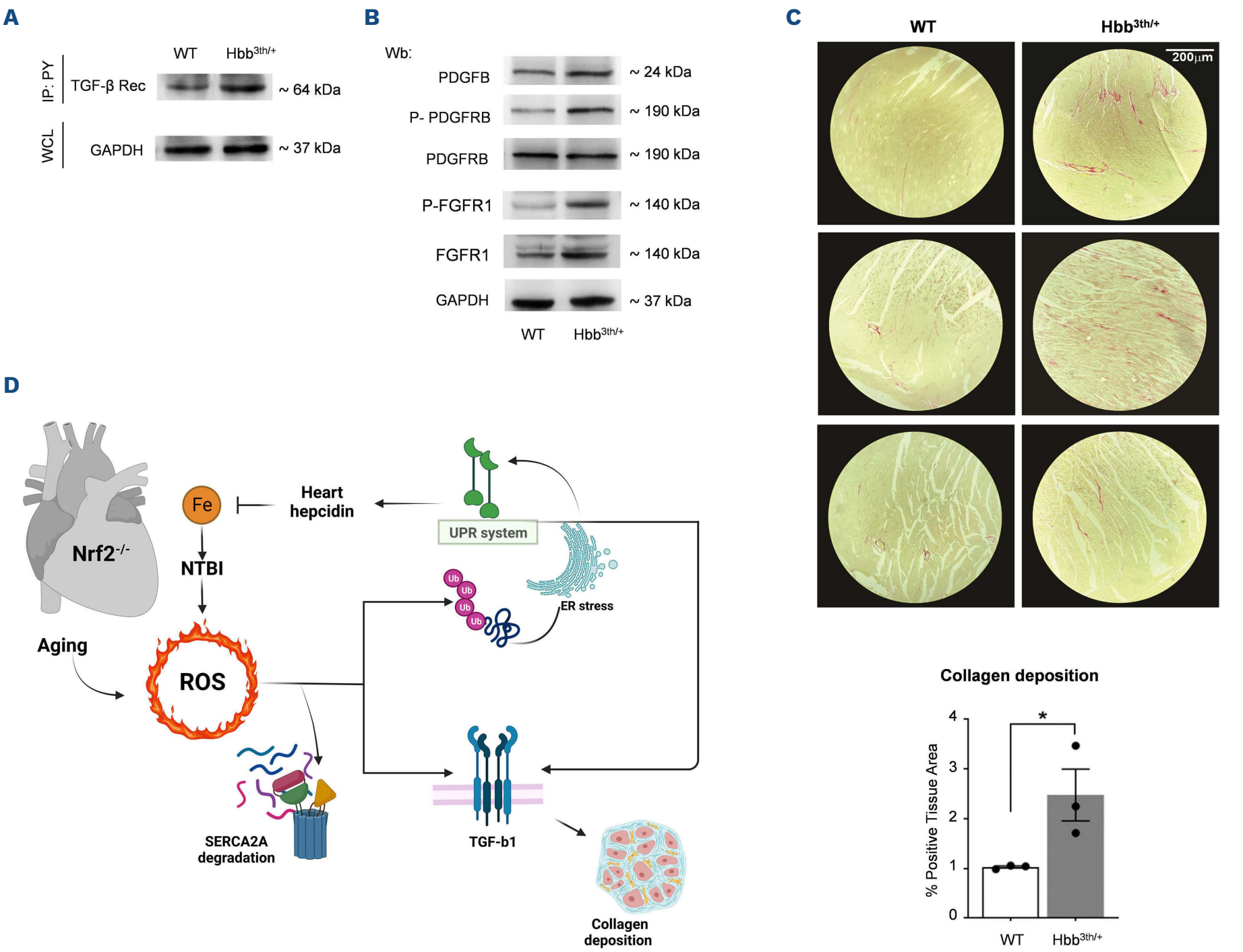

Figure 6. Activation of the TGF-β pathways and modulation of extracellular matrix remodeling factors characterize cardiomyopathy of β-thalassemic mice. (A) Heart immunoprecipitation using specific anti-phosphotyrosine antibodies (IP: pY), revealed with specific anti-TGF Receptor (Rec) antibody of 12-month-old WT and Hbbth3$^{/+}$ mice (n=4 for each group). GAPDH in whole-cell lysate (WCL) is used as loading control. One representative gel of 3 others with similar results is presented. Densitometric analysis of immunoblots is shown in *Online Supplementary Figure S10G*. (B) Immunoblot analysis, using specific antibodies against PDGF-B, phosphorylated (p-)PDGFR-B, PDGFR-B, p-FGFR1 and FGFR in the heart of 12-month-old WT and Hbbth3$^{/+}$ mice (n=4 for each group). GAPDH serves as protein loading control. One representative gel of 3 with similar results is shown. Densitometric analysis of immunoblots is shown in *Online Supplementary Figure S10H*. (C) Representative images of Picrosirius staining for collagen on heart sections of WT and Hbbth3$^{/+}$ mice (scale bars: 200 μm) and relative quantification expressed as percentage positive tissue area (n=3 for each group). (D) Schematic diagram of the dual role of Nrf2 in the development of age-dependent cardiomyopathy in the presence of iron overload diet. Nrf2 being a redox-related transcriptional factor it protects against age-dependent oxidation. The absence of Nrf2 (Nrf2$^{-/-}$ mice) results in an age-dependent cardiomyopathy, associated with severe oxidation (ROS: reactive oxygen species) and iron accumulation combined with increased non-transferrin bound iron (NTBI). These events favor (i) degradation of the sarcoplasmic reticulum calcium ATPase cardiac isoform 2 (SERCA2a), a calcium transport system important for myocardial performance; (ii) accumulation of polyubiquinated proteins and (iii) activation of transforming growth factor (TGF)-β pathways, promoting collagen deposition and cardiac fibrosis. In mice exposed to iron (Fe) overload diet, the absence of Nrf2 is paradoxically protective. Indeed, the sustained endoplasmic reticulum (ER) stress promotes overactivation of unfolded protein response (UPR) system. This results in upregulation of heart hepcidin, turning iron to accumulate in liver where the abnormality of Bmp2-6 pathway results in local impairment of Hamp synthesis.

novel evidence linking overactivation of the UPR system with hypertrophic cardiomyopathy in both IO Nrf2$^{-/-}$ and Hbb$^{th3/+}$ mice, opens a new perspective on cardiomyopathy in patients with β-thalassemia before the appearance of heart iron accumulation.

Disclosures

FV receives research funding from Silence Therapeutics, Vifor Pharma and PharmaNutra (none of them relevant to the current project). AG is the co-founder and scientific advisor of Kither Biotech, a pharmaceutical product company focused on respiratory medicine that is not in conflict with statements made in this article. All other authors have no conflicts of interest to disclose.

Contributions

EF, AM, FV, ET, AI and LDF designed the experiments, analyzed data and wrote the manuscript. EF, AM, II, SCM, AS and VR carried out immunoblot and protein analysis. SV carried out ferroportin analysis, NTBI and different heart staining. DB carried out Perls' staining and analyzed the data. IA carried out molecular analysis and wrote the manuscript. AG performed echocardiography, analyzed data and wrote the manuscript. MI and AL carried out the immune-microscopy on VCAM-1.

Acknowledgements

The authors would like to thank Rachele Perissinotto for preliminary results on MMP9 activity in heart from Nrf2$^{-/-}$ mice.

Funding

This study was founded by UNIVR-FUR to LDF.

Data-sharing statement

Please direct requests for original data to the corresponding author via email.

References

1. Wermke M, Eckoldt J, Gotze KS, et al. Enhanced labile plasma iron and outcome in acute myeloid leukaemia and myelodysplastic syndrome after allogeneic haemopoietic cell transplantation (ALLIVE): a prospective, multicentre, observational trial. Lancet Haematol. 2018;5(5):e201-e210.
2. Kumfu S, Fucharoen S, Chattipakorn SC, Chattipakorn N. Cardiac complications in beta-thalassemia: from mice to men. Exp Biol Med (Maywood). 2017;242(11):1126-1135.
3. Temraz S, Santini V, Musallam K, Taher A. Iron overload and chelation therapy in myelodysplastic syndromes. Crit Rev Oncol Hematol. 2014;91(1):64-73.
4. Kremastinos DT, Farmakis D. Iron overload cardiomyopathy in clinical practice. Circulation. 2011;124(20):2253-2263.
5. Dharmarajan K, Rich MW. Epidemiology, pathophysiology, and prognosis of heart failure in older adults. Heart Fail Clin. 2017;13(3):417-426.
6. Hershko C. Pathogenesis and management of iron toxicity in thalassemia. Ann N Y Acad Sci. 2010;1202:1-9.
7. Piga A, Longo F, Duca L, et al. High nontransferrin bound iron levels and heart disease in thalassemia major. Am J Hematol. 2009;84(1):29-33.
8. Ganz T. Systemic iron homeostasis. Physiol Rev. 2013;93(4):1721-1741.
9. Nemeth E, Tuttle MS, Powelson J, et al. Hepcidin regulates cellular iron efflux by binding to ferroportin and inducing its internalization. Science. 2004;306(5704):2090-2093.
10. van Breda GF, Bongartz LG, Zhuang W, et al. Cardiac hepcidin expression associates with injury independent of iron. Am J Nephrol. 2016;44(5):368-378.
11. Merle U, Fein E, Gehrke SG, Stremmel W, Kulaksiz H. The iron regulatory peptide hepcidin is expressed in the heart and regulated by hypoxia and inflammation. Endocrinology. 2007;148(6):2663-2668.
12. Mleczko-Sanecka K, Silvestri L. Cell-type-specific insights into iron regulatory processes. Am J Hematol. 2021;96(1):110-127.
13. Chen QM, Maltagliati AJ. Nrf2 at the heart of oxidative stress and cardiac protection. Physiol Genomics. 2018;50(2):77-97.
14. Liu Z, Han K, Huo X, et al. Nrf2 knockout dysregulates iron metabolism and increases the hemolysis through ROS in aging mice. Life Sci. 2020;255:117838.
15. De Franceschi L, Bertoldi M, Matte A, et al. Oxidative stress and beta-thalassemic erythroid cells behind the molecular defect. Oxid Med Cell Longev. 2013;2013:985210.
16. Li J, Zhang C, Xing Y, et al. Up-regulation of p27(kip1) contributes to Nrf2-mediated protection against angiotensin II-induced cardiac hypertrophy. Cardiovasc Res. 2011;90(2):315-324.
17. Wang H, Lai Y, Mathis BJ, et al. Deubiquitinating enzyme CYLD mediates pressure overload-induced cardiac maladaptive remodeling and dysfunction via downregulating Nrf2. J Mol Cell Cardiol. 2015;84:143-153.
18. Li J, Ichikawa T, Janicki JS, Cui T. Targeting the Nrf2 pathway against cardiovascular disease. Expert Opin Ther Targets. 2009;13(7):785-794.
19. Xing Y, Niu T, Wang W, et al. Triterpenoid dihydro-CDDO-trifluoroethyl amide protects against maladaptive cardiac remodeling and dysfunction in mice: a critical role of Nrf2. PLoS One. 2012;7(9):e44899.
20. Lim PJ, Duarte TL, Arezes J, et al. Nrf2 controls iron homeostasis in haemochromatosis and thalassaemia via Bmp6 and hepcidin. Nat Metab. 2019;1(5):519-531.
21. Matte A, De Falco L, Iolascon A, et al. The interplay between peroxiredoxin-2 and nuclear factor-erythroid 2 is important in limiting oxidative mediated dysfunction in beta-thalassemic erythropoiesis. Antioxid Redox Signal. 2015;23(16):1284-1297.
22. Kerins MJ, Ooi A. The roles of NRF2 in modulating cellular iron homeostasis. Antioxid Redox Signal. 2018;29(17):1756-1773.
23. Fang X, Wang H, Han D, et al. Ferroptosis as a target for protection against cardiomyopathy. Proc Natl Acad Sci U S A. 2019;116(7):2672-2680.
24. Matte A, De Falco L, Federti E, et al. Peroxiredoxin-2: a novel regulator of iron homeostasis in ineffective erythropoiesis. Antioxid Redox Signal. 2018;28(1):1-14.
25. Schnelle M, Catibog N, Zhang M, et al. Echocardiographic evaluation of diastolic function in mouse models of heart disease. J Mol Cell Cardiol. 2018;114:20-28.

26. Vinchi F, Porto G, Simmelbauer A, et al. Atherosclerosis is aggravated by iron overload and ameliorated by dietary and pharmacological iron restriction. Eur Heart J. 2020;41(28):2681-2695.
27. Andolfo I, Rosato BE, Manna F, et al. Gain-of-function mutations in PIEZO1 directly impair hepatic iron metabolism via the inhibition of the BMP/SMADs pathway. Am J Hematol. 2020;95(2):188-197.
28. Matte A, Recchiuti A, Federti E, et al. Resolution of sickle cell disease-associated inflammation and tissue damage with 17R-resolvin D1. Blood. 2019;133(3):252-265.
29. Federti E, Matte A, Ghigo A, et al. Peroxiredoxin-2 plays a pivotal role as multimodal cytoprotector in the early phase of pulmonary hypertension. Free Radic Biol Med. 2017;112:376-386.
30. Vinchi F, De Franceschi L, Ghigo A, et al. Hemopexin therapy improves cardiovascular function by preventing heme-induced endothelial toxicity in mouse models of hemolytic diseases. Circulation. 2013;127(12):1317-1329.
31. Roczkowsky A, Chan BYH, Lee TYT, et al. Myocardial MMP-2 contributes to SERCA2a proteolysis during cardiac ischaemia-reperfusion injury. Cardiovasc Res. 2020;116(5):1021-1031.
32. Schmidt PJ, Racie T, Westerman M, et al. Combination therapy with a Tmprss6 RNAi-therapeutic and the oral iron chelator deferiprone additively diminishes secondary iron overload in a mouse model of beta-thalassemia intermedia. Am J Hematol. 2015;90(4):310-313.
33. Erkens R, Kramer CM, Luckstadt W, et al. Left ventricular diastolic dysfunction in Nrf2 knock out mice is associated with cardiac hypertrophy, decreased expression of SERCA2a, and preserved endothelial function. Free Radic Biol Med. 2015;89:906-917.
34. Zhang C, Wang Y, Ge Z, et al. GDF11 Attenuated ANG II-induced hypertrophic cardiomyopathy and expression of ANP, BNP and beta-MHC through down-regulating CCL11 in mice. Curr Mol Med. 2018;18(10):661-671.
35. Cao X, Mao M, Diao J, et al. Ectopic Overexpression of PPARgamma2 in the heart determines differences in hypertrophic cardiomyopathy after treatment with different thiazolidinediones in a mouse model of diabetes. Front Pharmacol. 2021;12:683156.
36. Temsah RM, Netticadan T, Chapman D, et al. Alterations in sarcoplasmic reticulum function and gene expression in ischemic-reperfused rat heart. Am J Physiol. 1999;277(2):H584-594.
37. French JP, Quindry JC, Falk DJ, et al. Ischemia-reperfusion-induced calpain activation and SERCA2a degradation are attenuated by exercise training and calpain inhibition. Am J Physiol Heart Circ Physiol. 2006;290(1):H128-136.
38. Das SK, Wang W, Zhabyeyev P, et al. Iron-overload injury and cardiomyopathy in acquired and genetic models is attenuated by resveratrol therapy. Sci Rep. 2015;5:18132.
39. Silveira C, Campos DHS, Freire PP, et al. Importance of SERCA2a on early isolated diastolic dysfunction induced by supravalvular aortic stenosis in rats. Braz J Med Biol Res. 2017;50(5):e5742.
40. Tsika RW, Ma L, Kehat I, et al. TEAD-1 overexpression in the mouse heart promotes an age-dependent heart dysfunction. J Biol Chem. 2010;285(18):13721-13735.
41. Neef S, Maier LS. Novel aspects of excitation-contraction coupling in heart failure. Basic Res Cardiol. 2013;108(4):360.
42. Prathipati P, Metreveli N, Nandi SS, Tyagi SC, Mishra PK. Ablation of matrix metalloproteinase-9 prevents cardiomyocytes contractile dysfunction in diabetics. Front Physiol. 2016;7:93.
43. Yadav SK, Kambis TN, Kar S, Park SY, Mishra PK. MMP9 mediates acute hyperglycemia-induced human cardiac stem cell death by upregulating apoptosis and pyroptosis in vitro. Cell Death Dis. 2020;11(3):186.
44. Iwabuchi M, Sheng H, Thompson JW, et al. Characterization of the ubiquitin-modified proteome regulated by transient forebrain ischemia. J Cereb Blood Flow Metab. 2014;34(3):425-432.
45. Sato Y, Kobayashi H, Sato S, et al. Systemic accumulation of undigested lysosomal metabolites in an autopsy case of mucolipidosis type II; autophagic dysfunction in cardiomyocyte. Mol Genet Metab. 2014;112(3):224-228.
46. Peikert K, Federti E, Matte A, et al. Therapeutic targeting of Lyn kinase to treat chorea-acanthocytosis. Acta Neuropathol Commun. 2021;9(1):81.
47. Zhai X, Wang W, Sun S, et al. 4-Hydroxy-2-nonenal promotes cardiomyocyte necroptosis via stabilizing receptor-interacting serine/threonine-protein kinase 1. Front Cell Dev Biol. 2021;9:721795.
48. Lu J, Sun B, Huo R, et al. Bone morphogenetic protein-2 antagonizes bone morphogenetic protein-4 induced cardiomyocyte hypertrophy and apoptosis. J Cell Physiol. 2014;229(10):1503-1510.
49. Aschemeyer S, Qiao B, Stefanova D, et al. Structure-function analysis of ferroportin defines the binding site and an alternative mechanism of action of hepcidin. Blood. 2018;131(8):899-910.
50. Li J, Ichikawa T, Villacorta L, et al. Nrf2 protects against maladaptive cardiac responses to hemodynamic stress. Arterioscler Thromb Vasc Biol. 2009;29(11):1843-1850.
51. Nian M, Lee P, Khaper N, Liu P. Inflammatory cytokines and postmyocardial infarction remodeling. Circ Res. 2004;94(12):1543-1553.
52. Ge C, Hu L, Lou D, et al. Nrf2 deficiency aggravates PM2.5-induced cardiomyopathy by enhancing oxidative stress, fibrosis and inflammation via RIPK3-regulated mitochondrial disorder. Aging (Albany NY). 2020;12(6):4836-4865.
53. Szostek-Mioduchowska AZ, Lukasik K, Skarzynski DJ, Okuda K. Effect of transforming growth factor -beta1 on alpha-smooth muscle actin and collagen expression in equine endometrial fibroblasts. Theriogenology. 2019;124:9-17.
54. Gallini R, Lindblom P, Bondjers C, Betsholtz C, Andrae J. PDGF-A and PDGF-B induces cardiac fibrosis in transgenic mice. Exp Cell Res. 2016;349(2):282-290.
55. Kalra K, Eberhard J, Farbehi N, Chong JJ, Xaymardan M. Role of PDGF-A/B ligands in cardiac repair after myocardial infarction. Front Cell Dev Biol. 2021;9:669188.
56. Vecchi C, Montosi G, Zhang K, et al. ER stress controls iron metabolism through induction of hepcidin. Science. 2009;325(5942):877-880.
57. Lee JM. Nuclear receptors resolve endoplasmic reticulum stress to improve hepatic insulin resistance. Diabetes Metab J. 2017;41(1):10-19.
58. Minakshi R, Rahman S, Jan AT, Archana A, Kim J. Implications of aging and the endoplasmic reticulum unfolded protein response on the molecular modality of breast cancer. Exp Mol Med. 2017;49(11):e389.
59. Dickhout JG, Carlisle RE, Austin RC. Interrelationship between cardiac hypertrophy, heart failure, and chronic kidney disease: endoplasmic reticulum stress as a mediator of pathogenesis. Circ Res. 2011;108(5):629-642.
60. Tanjore H, Lawson WE, Blackwell TS. Endoplasmic reticulum stress as a pro-fibrotic stimulus. Biochim Biophys Acta. 2013;1832(7):940-947.
61. Chinprateep B, Ratanasit N, Kaolawanich Y, et al. Prevalence of left ventricular diastolic dysfunction by cardiac magnetic resonance imaging in thalassemia major patients with normal left ventricular systolic function. BMC Cardiovasc Disord.

2019;19(1):245.
62. Spirito P, Lupi G, Melevendi C, Vecchio C. Restrictive diastolic abnormalities identified by Doppler echocardiography in patients with thalassemia major. Circulation. 1990;82(1):88-94.
63. Korf-Klingebiel M, Kempf T, Schluter KD, et al. Conditional transgenic expression of fibroblast growth factor 9 in the adult mouse heart reduces heart failure mortality after myocardial infarction. Circulation. 2011;123(5):504-514.
64. Murphy CJ, Oudit GY. Iron-overload cardiomyopathy: pathophysiology, diagnosis, and treatment. J Card Fail. 2010;16(11):888-900.
65. Gu J, Cheng Y, Wu H, et al. Metallothionein is downstream of Nrf2 and partially mediates sulforaphane prevention of diabetic cardiomyopathy. Diabetes. 2017;66(2):529-542.
66. Tian C, Gao L, Zucker IH. Regulation of Nrf2 signaling pathway in heart failure: Role of extracellular vesicles and non-coding RNAs. Free Radic Biol Med. 2021;167:218-231.
67. Maejima Y. The critical roles of protein quality control systems in the pathogenesis of heart failure. J Cardiol. 2020;75(3):219-227.
68. Gotoh T, Oyadomari S, Mori K, Mori M. Nitric oxide-induced apoptosis in RAW 264.7 macrophages is mediated by endoplasmic reticulum stress pathway involving ATF6 and CHOP. J Biol Chem. 2002;277(14):12343-12350.
69. Lenna S, Trojanowska M. The role of endoplasmic reticulum stress and the unfolded protein response in fibrosis. Curr Opin Rheumatol. 2012;24(6):663-668.
70. Nakada EM, Sun R, Fujii U, Martin JG. The impact of endoplasmic reticulum-associated protein modifications, folding and degradation on lung structure and function. Front Physiol. 2021;12:665622.